

Velocity structure of the dwarf galaxy population in the Centaurus cluster

P. Stein¹, H. Jerjen², and M. Federspiel³

¹ Departament d'Astronomia i Meteorologia, Universitat de Barcelona, Avenida Diagonal 647, E-08028 Barcelona, Spain. E-mail: paul@pcess2.am.ub.es

² Mt. Stromlo and Siding Spring Observatories, Australian National University, Private Bag, Weston Creek PO, ACT 2611, Canberra, Australia. E-mail: jerjen@mso.anu.edu.au

³ Astronomisches Institut der Universität Basel, Venusstrasse 7, CH-4102 Binningen, Switzerland. E-mail: federspiel@ubaclu.unibas.ch

the date of receipt and acceptance should be inserted later

Abstract. Based on the photometric survey of the inner region of the Centaurus cluster (Jerjen & Dressler 1997a) we measured redshifts for a deep, surface brightness limited sample of galaxies using the MEFOS multifibre spectrograph at the ESO 3.6m telescope. With the new data set radial velocities for 120 centrally located cluster members become available which is equivalent to 78% of all known cluster galaxies in the region brighter than $B_T=18.5$. The relevant aspect of this investigation is that new redshifts for 32 dwarf galaxies have been measured, rising the total number to 48. We investigate the prominent bimodal velocity distribution of Centaurus in more detail, discussing the very different characteristics of the velocity distributions for the main Hubble types E&S0, spirals, Im&BCD, and dE&dS0. The nucleated, bright dwarf ellipticals are the only galaxies with a Gaussian-like distribution centred at $3148 \pm 98 \text{ km s}^{-1}$. The remarkable coincidence of this velocity with the mean velocity of Cen30 and the redshift of NGC 4696 in particular strongly suggests a connection of the dE&dS0s to the gravitational centre of the Centaurus cluster and/or to the cluster dominant E galaxy. The application of statistical tests reveals the existence of a population dwarf galaxies bound to NGC 4696. The dynamical parameters for the two velocity components suggest that Cen30 is the real Centaurus cluster whereas Cen45 can only be a loosely bound group of galaxies. This conclusion is followed up with a type-mixture analysis. All results are fully consistent with the cluster-group scenario. Whether Cen45 is merging with the cluster or is located in the close background remains unclear. We show that the poorness of Cen45 represents an intrinsic problem which makes it difficult to approach this question.

Key words: cosmology – clusters of galaxies: individual – evolution of – galaxies: redshifts – dwarf – giant – evolution of

1. Introduction

Lucey et al. (1986a, hereafter LCD) discovered a remarkable bimodal velocity distribution for the classical Hubble types E, S0, and spirals in the Centaurus cluster. The two velocity components were found to be roughly centred at 3000 km s^{-1} and 4500 km s^{-1} and were denoted as Cen30 and Cen45, respectively. Two fundamentally different scenarios have been suggested to explain the phenomenon. (1) Centaurus may be just a superposition of two spatially separated clusters at relative distances to Virgo of 1.67 and 2.38, respectively (Lynden-Bell et al. 1988, Faber et al. 1989). If true, large peculiar velocities for the two clusters would be the consequence in good agreement with the large-scale streaming motion of nearby galaxies towards the "Great Attractor" (Dressler et al. 1987, Lynden-Bell et al. 1988), a large concentration of mass $\sim 5 \cdot 10^{16} M_\odot$ with its gravitational potential well close to the galaxy cluster Abell 3627, as was discovered recently by Kraan-Korteweg et al. (1996). (2) A less spectacular but equally attractive explanation for the bimodality is that we are dealing with a young, dynamically unrelaxed galaxy cluster consisting of two unequal subclumps (Lucey & Carter 1988, hereafter LC). The less massive component Cen45 is about to merge with the main cluster component Cen30 and the large velocity difference of $\sim 1500 \text{ km s}^{-1}$ for the components is interpreted as due to the gravitational infall of Cen45 into the major cluster centre. Although some new results have been published on the Centaurus cluster recently (Dressler 1993; Jerjen 1995; Jerjen & Dressler 1997b), a conclusive explanation for the origin of the bimodal velocity distribution could not yet be given. Centaurus is the closest galaxy cluster to the Local Group showing this kind of feature and thus the best candidate to explore such a phenomenon. A clarification of the situation is highly desirable for a better understanding of structure formation in the Universe on the scale of galaxy clusters as well as on larger scales such as the proposed "Great Attractor" supercluster.

Moreover, there is another challenge offered by the Centaurus cluster. From kinematical studies of the clusters in Virgo (Binggeli et al. 1993) and Fornax (Held & Mould 1994) we

* Based on observations made at the European Southern Observatory, La Silla, Chile.

Send offprint requests to: M. Federspiel (Universität Basel)

know that the velocity distribution of early-type dwarfs might differ significantly from that of the giants. This could be due to cluster formation effects and/or evolution of dwarf galaxies in high density environments. In particular, the observed clumpiness of low density regions in galaxy clusters and the marked spatial and velocity segregation of galaxy types (e.g. Stein 1997) suggest the occurrence of significant late infall of spiral galaxies from the cluster outskirts onto the core (Binggeli et al. 1987). These infalling late-type galaxies are likely to be initially surrounded by a bound population of dwarf satellites, as was found to be the case for the field (Vader & Sandage 1991). It seems to be clear that a significant fraction of bound (dwarf) galaxies can be found in clusters (Ferguson 1992), but it is still not known whether all reach the central cluster region as companions of spirals or whether there are other evolutionary effects involved. It has been proposed to extract dynamical information about a cluster using dwarf galaxies as test particles in the cluster potential well (Binggeli et al. 1987), given that their gravitational pull on neighbouring giant galaxies is negligible. In the case of relaxed clusters with a central dominant galaxy up to 5% of the cluster members were found to be possibly bound to the central system (Gebhardt & Beers 1991; Merrifield & Kent 1991; but see Blakeslee & Tonry 1992). So far the only studies about bound populations involving distinctions between dwarf and giant galaxies have been Ferguson's (1992) and Binggeli's (1993) analysis of the Virgo cluster.

The aim of the present study is to explore the velocity distributions of different galaxy types in the Centaurus cluster with special weight on the dwarf families. This shall help to give us more insight into the kinematic properties of this complex galaxy aggregation and of type-dependent cluster dynamics in general.

The sample selection is discussed in Sect. 2. A technical description of the spectroscopic observations and of the data reduction follows in Sect. 3. The resulting new redshifts were then used to check the validity of previous membership assignments based on morphological information alone (Sect. 4). We present our analysis of the data in Sections 5 and 6, where type-dependent velocity distributions are interpreted and the existence of bound galaxies is investigated. Main results are summarized in Sect. 7.

2. Sample selection

With the deep photometric Centaurus cluster survey (Jerjen 1995) an extensive list of new cluster dwarf galaxies became available including accurate positions and high morphological resolution. These latter quantities are based on a fine-scale 20-inch Las Campanas du Pont plate covering the central 1.5×1.5 degrees of the cluster. The probability of cluster membership was worked out based on pure morphological criteria and is given as 50% or higher for each galaxy included in the catalogue. For our redshift project we selected all galaxies of the outgoing Centaurus cluster catalogue (Jerjen & Dressler 1997a, hereafter CCC) with a mean effective B -band surface brightness SB_{eff} brighter than $25.0 \text{ mag arcsec}^{-2}$. This implies our

sample contains a substantial number of newly discovered dwarf galaxies as well as several mainly giant galaxies with known redshifts (Dickens et al. 1986, hereafter DCL; LC; Stein 1996). The latter subsample was used for comparison.

The restriction of our redshift survey onto the inner region of the Centaurus cluster was not only dictated by the area of the photometric survey but is also required to overcome uncontrollable cluster sample contamination by unrelated galaxies located at a Hubble distance of $\sim 4500 \text{ km s}^{-1}$. In fact, this is a crucial problem for the Centaurus cluster as already emphasized elsewhere (Lucey et al. 1986b).

3. Observations and data reduction

Observations were carried out between May 23–26, 1995 at the 3.6 m ESO telescope at La Silla. We employed the multi-fibre instrument MEFOS, which has a circular field of view of 1 degree and 29 fibre arms. Each arm carries one image fibre of $36 \times 36 \text{ arcsec}$ and two spectral fibres of 2.5 arcsec aperture for simultaneous object and sky acquisition. The image fibre is meant for the interactive repositioning of spectral fibres onto the object of choice, prior to the spectral exposure. For a detailed study about the performance of MEFOS consult Felenbok et al. 1997.

No beam-switching technique has been applied for subtraction of the night sky spectral contribution (Cuby & Mignoli 1994), because the traditional technique with fibre transmission correction (given by the signal under the OI emission line at 5577.4 \AA) gave suitable results. The 512 pixels of the CCD covered the wavelength range 3800 to 6100 \AA . A total exposure time between 5400 and 7200 s per field was chosen.

Reduction of the spectroscopic data was done using the MIDAS package on an IBM AIX/RS6000. All frames were carefully corrected for pixel-to-pixel variations in sensitivity (flat-fielded). Then an optimal extraction algorithm was applied (Horne 1986), which was able to correct for most of the cosmic ray hits. No correction for stray light nor cross-talk between fibres (Lissandrini et al. 1994) was applied, because it could have influenced the precision of the optimal extraction. The resulting one-dimensional spectra were then calibrated in wavelength and the positions of night-sky emission lines were checked against their expected wavelength. Note that no appreciable systematic deviation in the position of night-sky lines was found, as opposed to the findings of Felenbok et al. 1997, who comment on their problems with observations taken roughly one year before us.

Prior to sky subtraction the signal of each spectrum (including sky spectra) had to be scaled with respect to the intrinsic transmission efficiency of the corresponding fibre. To determine the transmission efficiency of each fibre the signal under the 5577.4 \AA night-sky line was used, taking an average for each fibre over all observed fields. Creation of a mean sky spectrum was done taking all available sky spectra from the corresponding pair of exposures.

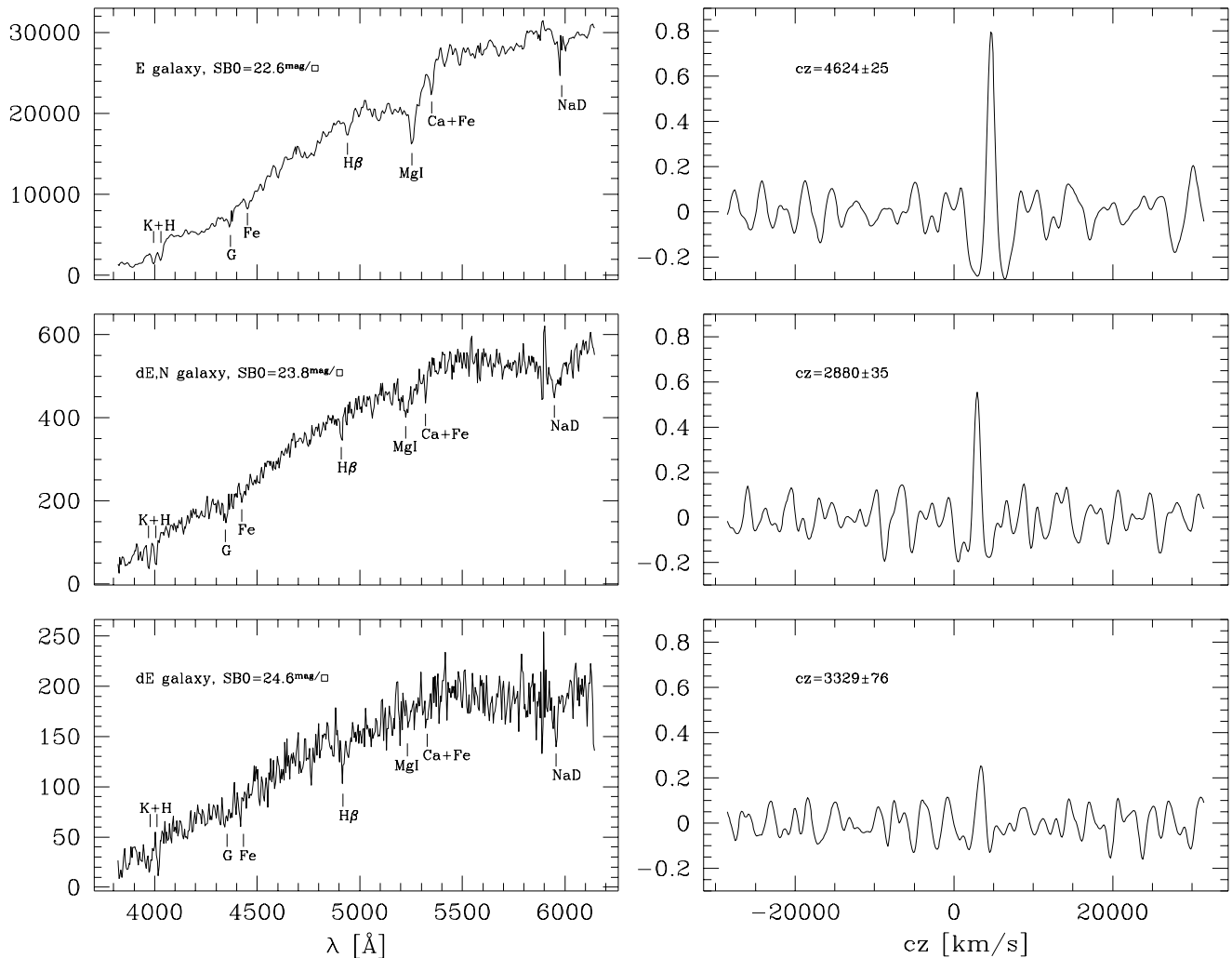


Fig. 1. Typical spectra and their cross-correlation functions. The uppermost spectrum belongs to NGC 4709, the dominant galaxy of Cen45. Note the good symmetry in the correlation function around its peak. At the bottom a very low-surface brightness galaxy is shown, for which a redshift measurement was at the limit of feasibility. The inferred positions of some of the main absorption lines are marked.

3.1. Emission-line redshifts

First, those galaxies were selected which had at least two clearly visible emission lines, mostly OII, $H\beta$ and OIII. A Gaussian superposed onto a quadratic polynomial was then used to fit each line interactively. The final emission line redshift was computed as the unweighted mean over all N emission lines present in one galaxy spectrum. Errors in each measurement were taken to be 100 km s^{-1} , independently of line strength, because the main factor of uncertainty involved had been found to be the wavelength calibration (Stein 1996). Thus, the errors of the emission line redshifts are taken as $100/\sqrt{N}$.

3.2. Cross-correlation redshifts

Prior to cross-correlation redshift measurements, residual features around the positions of strong night-sky lines had to be re-

moved, as well as all galaxy emission lines. Next, a procedure of spectra preparation was followed which was virtually the same as described in Tonry & Davis (1979). See Stein (1996) for details about template selection. Typical spectra and peaks of the obtained cross-correlation functions are shown in Fig. 1.

Table 1 lists the efficiency (number of redshifts obtained/number of observed galaxies) of the instrument together with the reduction procedure up to a given limiting effective surface brightness, as well as the corresponding limiting apparent total magnitude for point-like sources. The latter quantity was estimated taking into consideration the fibre radius of 1.25 arcsec, and under the assumption of an exponential surface brightness profile, a mean scale length of 2.9 arcsec, a mean effective radius of 3.6 arcsec (Jerjen & Dressler 1997a) and for the case that the fibre had been ideally centred onto the galaxy. Two fields were excluded from the analysis because of their much lower yield due to problems with the autoguider.

SB_{eff} (1)	B_T (2)	efficiency (3)
< 23.0	< 20.4	100 %
23.0 – 23.5	20.4 – 20.9	100 %
23.5 – 24.0	20.9 – 21.4	84 %
24.0 – 24.5	21.4 – 21.9	73 %
24.5 – 25.0	21.9 – 22.4	26 %

Table 1. Efficiency in redshift determination for galaxies of different effective surface brightnesses. For comparison purposes, the hypothetical B magnitude of a point-like source which on the average would feed the fibres with the same amount of light is also given. Optimal positioning of the fibres is hereby assumed.

The limit in surface brightness which could be reached here confirms that projects aiming at the systematic measurement of redshifts for dwarf galaxies in nearby clusters are feasible, even with a multi-fibre instrument. The only requirement is a large field of view.

3.3. Scaling and checking the data

Correction for the earth motion was then carried out, leading to heliocentric corrected redshifts for both the cross-correlation and the emission-line redshifts.

For 32 galaxies the redshifts obtained here could be compared to those obtained previously by one of us (Stein 1996). Note that cross-correlation errors for the brightest galaxies in Stein (1996) might be slight underestimations, due to the fact that the template had been constructed using a sample of these same bright galaxies. Thus, the scaling factor between internal (Tonry & Davis 1979) and external errors is determined using only galaxies in the calibration sample with errors of 20 km s^{-1} or above. With an error scaling factor of 1.7 the differences between redshifts in both datasets are perfectly consistent with the resulting external errors. A zero-point shift of 26 km s^{-1} was then applied to the cross-correlation data.

Only for six galaxies it was possible to obtain both cross-correlation and emission-line redshifts. Again, the distribution of differences is in good agreement with the expectations, given the uncertainties in both measurements. Finally, a weighted mean of emission and absorption (cross-correlation) redshifts was taken.

4. Membership: morphology versus redshift

We measured redshifts for 115 galaxies. The data are listed in Tables 5a, 5b, and 5c combined with data from the CCC such as morphological type, total apparent B magnitude, and SB_{eff} . Galaxies with no previous redshift measurement are subdivided into two lists according to cluster members (Table 5a)

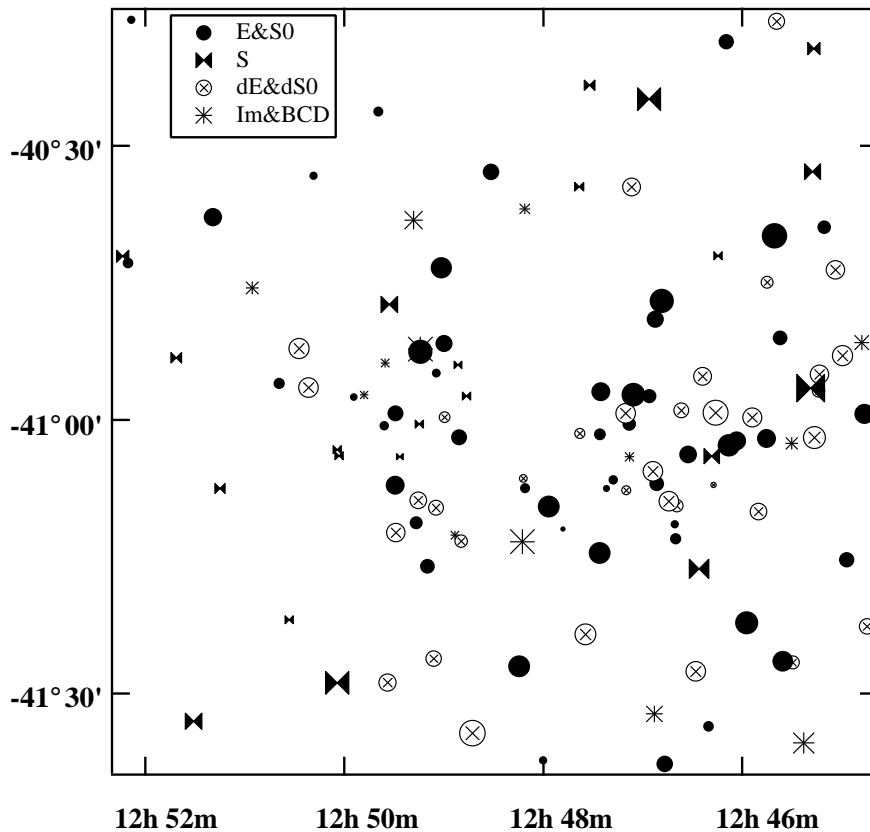
and background objects (Table 5b). Table 5c contains the data for galaxies which already had a redshift measured and are confirmed cluster members.

Among our galaxies there are 101 with velocities smaller than 5414 km s^{-1} . This velocity corresponds to the 3σ upper limit for the velocity distribution of Cen45 (LCD) and was used as a cut-off to discriminate between cluster members and background galaxies. Actually, the remaining 14 velocities lie between $10\,000$ and $38\,000 \text{ km s}^{-1}$ which makes a separation unambiguous. Our cluster sample was complemented by 19 redshifts taken from the literature (DCL; LC; Stein 1996). Finally, the dataset upon which the following analysis is based consists of redshifts for 120 cluster members located in the central cluster area. A weighted average was taken in case of multiple redshifts, after homogenization of zero-point-shifts and scaling of errors among the four sources. The completeness of this data set is very high with respect to apparent magnitude and effective surface brightness. Redshifts are available for 96 percent of all known cluster galaxies brighter than $B_T=17.5$. At the limit of $B_T=18.5$ our redshift sample is still complete to 78 percent. This latter magnitude corresponds to $M_{B_T} = -15.3$, assuming a cluster distance modulus of $(m - M)_{\text{Cen}}=33.79$ (Jerjen & Dressler 1997b) and including an extinction term of $A_B=0.42$. For SB_{eff} the completeness levels are 93 percent at $23.5 B \text{ arcsec}^{-2}$ and 78 percent at $24.5 B \text{ arcsec}^{-2}$, respectively.

Tables 5a and 5b contain data for 50 galaxies with new measured velocities among which 36 galaxies are cluster members according to our selection criterion. Their Hubble type mixture is (E&S0/S/Im&BCD/dE&dS0) = (1/3/11/21). The composition of the background sample is (0/3/6/5). For the latter sample the morphological information may not necessarily be true any more because the classification had been done under the assumption of cluster membership. The new measured redshifts shall be used to estimate the accuracy of the morphological based cluster membership for dwarf galaxies in the CCC. For this purpose we compare in Table 2 the number of cluster members and background objects for the two dwarf families individually. In column 1 we give the three membership classes as listed in the CCC. Columns 2 and 3 give the observed numbers of late-type dwarfs of a particular membership class divided into members (m) and background (b) according to their redshifts. From columns 2 and 3 we derive the fraction of real cluster members in column 4 which can be compared to the percentages listed in column 1. The same analysis is done for the early-type dwarfs in the columns 5–7. As can be seen, the numbers in columns 1, 4 and 7 are in good agreement. The 100% case is slightly overestimated (what one naturally would expect) whereas the 75% case is clearly underestimated. Combining class 1 and 2, the membership assignment has a success rate of 90% for both dwarf families. Overall, these results strongly support the idea that morphological criteria are an excellent tool to discriminate between cluster and background galaxies even for clusters at the distance of Centaurus if one works with high resolution material and spatially well isolated clusters.

Table 2. Morphological membership assignment compared to redshift data (explanation see text)

membership (morph)	m	Im&BCD		membership (redshift)	m	dE&dS0	
		b	membership (redshift)			b	membership (redshift)
(1)	(2)	(3)	(4)	(5)	(6)	(7)	
1=	100%	7	1	88%	14	2	88%
2=	75%	1	0	100%	3	0	100%
3=	50%	3	5	38%	4	3	57%

**Fig. 2.** A map of all Centaurus cluster member galaxies with known redshifts. The symbol size is inversely proportional to the redshift.

5. Velocity distributions

An illustration of the 3D distribution of the Centaurus galaxies is given in Fig. 2 using the two coordinates and radial velocity. In projection, Centaurus shows a pronounced bimodal substructure along the East-West direction. At $RA \sim 12^{\text{h}}48^{\text{m}}30^{\text{s}}$ a vertical void in the galaxy distribution separates the two cluster subclumps. The significance of this so-called Centaurus Gap is shown based on Lee statistics and Monte Carlo cluster models (Jerjen 1997). The large Western clump is mostly populated with early-type galaxies and dominated by the brightest cluster member, the E/S0 galaxy NGC 4696 at a velocity $2961 \pm 26 \text{ km s}^{-1}$ (weighted mean of three sources). The late-type galaxies can be found preferentially in the smaller Eastern concentration which leads to a morphological segregation in the 2D distribution for giants (LCD) and dwarfs described in detail by Jerjen (1995). But it is obvious that the morphological mixture

also varies as a function of redshift. The low velocity range (large symbols in the plot) is governed by early-type galaxies. Going to higher redshifts (small symbols) the mixture changes in favour of spirals and Im&BCDs.

This morphological segregation with redshift becomes clearer when focusing onto the radial velocity information only. Fig. 3 shows the velocity distributions for giants, dwarfs, and for the complete sample binned into 200 km s^{-1} intervals. Dwarfs and giants both exhibit irregular shapes which appear to be totally incompatible. An explanation for these puzzling distributions will be found thanks to the better morphological resolution we have for our sample (see Fig. 4 below). Only the giant galaxy sample shows a weak indication for a bimodality which is highly amplified by the dwarfs in the combined sample. To quantify the bimodal structure of the giant and complete samples we fitted a double Gaussian function to the data. The total number of sample galaxies was kept fixed and the errors

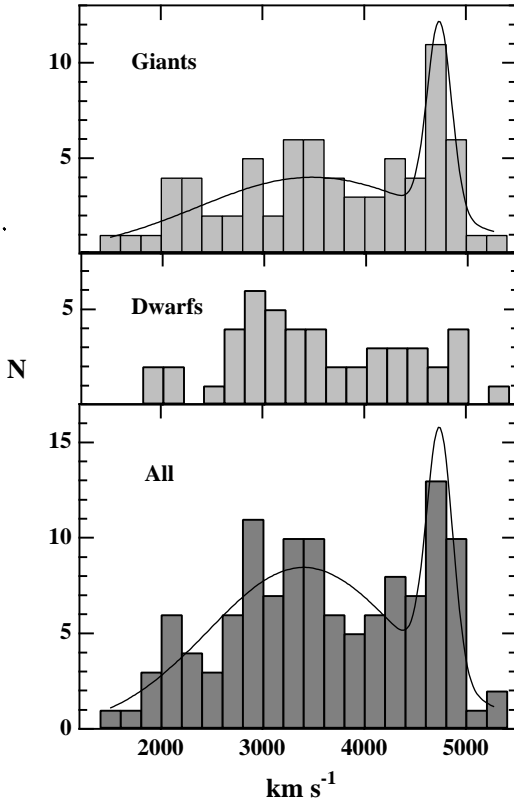


Fig. 3. The velocity distributions for the giant, the dwarf and the combined sample. Solid lines represent the best fitting double Gaussian functions.

were assumed to be \sqrt{N} . The best-fitting parameters are listed in Table 3. Both parameter sets are in good agreement but are slightly different from the estimates of LCD. Their cluster parameters have been included for comparison. They were derived from a $< 1^\circ$ sample of giant galaxies complete down to $G_{26.5} = 16.5$. Definitely, the parameter which discriminates best between the two velocity components is their richness, i.e. the number of galaxies assigned to each component at our completeness level in mean surface brightness. The ratio $n_{30}/n_{45}=4.7$ gives a clear hint to the different nature of Cen30 and Cen45. Cen30 is much richer in galaxies and appears as a typical galaxy cluster when its large velocity dispersion of $933 \pm 118 \text{ km s}^{-1}$ is compared to the velocity dispersion distribution for Abell clusters (Girardi et al. 1993). On the other hand, the first conclusion to be drawn from the very low value for σ_{45} is that Cen45 can only be a loosely bound system. A galaxy group seems to be a much better picture for this velocity component rather than a cluster. We like to emphasize that these results are based on pure statistical and dynamical arguments and therefore independent from the underlying spatial structure of the Centaurus cluster.

Our first conclusion about the nature of the galaxy aggregations Cen30 and Cen45 predicts a difference in the galaxy type-mixture taking into account the morphology-density rela-

Table 3. Best parameters for the double Gaussian fit

	Giants	Early types ($r < 0.75^\circ$)	All	Giants (LCD) ($r < 1^\circ$)
n_{30}	57 ± 5	62 ± 10	99 ± 7	
μ_{30}	3491 ± 225	3170 ± 174	3397 ± 139	3130
σ_{30}	1135 ± 200	738 ± 175	933 ± 118	780
n_{45}	15 ± 5	11.5 ± 10	21 ± 7	
μ_{45}	4741 ± 45	4788 ± 154	4746 ± 43	4634
σ_{45}	120 ± 41	345 ± 144	131 ± 43	260
χ^2	7.8	5.4	10.1	

tion for giants (Dressler 1980) and dwarfs (Binggeli et al. 1987; Ferguson & Sandage 1988; Binggeli et al. 1990). A higher fraction of early-type galaxies is expected in Cen30 than in Cen45 which shall be examined. Due to the overlapping Gaussian profiles it is not possible to associate all individual galaxies to one particular component. However, we can employ the best fitting pair of Gaussian profiles from the complete galaxy sample to determine the probability of each galaxy to be member of one particular component. Tables 5a and 5c contain the column prob_{45} which gives the probability of being a Cen45 member. A value of 0.00 implies a 100% probability of being a Cen30 member. Therefrom we calculate statistically the type-mixtures which are shown in Table 4. As expected, Cen30 is much richer in early-type galaxies than Cen45 with a 74% portion as compared to 48%. In order to understand the prominent difference in the early to late-type dwarf ratio (dE&dS0/Im&BCD) which is 3.6 for Cen30 and 0.5 for Cen45, respectively, one has to remember that the brightest dE&dS0s can be found only in clusters or as close companions to massive parent galaxies. In fact, all known dE&dS0s brighter than about $M_{BT} = -16$ are cluster members. For instance, the brightest dE&dS0s in Virgo, Fornax, or Centaurus are -18 (Sandage et al. 1985), -17.5 (Ferguson & Sandage 1988), and -18 (Jerjen & Tammann 1997), respectively. On the other hand, NGC 205 is the brightest dwarf elliptical in the LG with only $M_{BT} = -15.6$ and the nearby Cen A group has no dwarf brighter than $M_{BT} = -13$ (Jerjen et al. 1997). Our completeness limit is about $M_{BT} \sim -15.5$. Therefore, the dE&dS0/Im&BCD ratio is naturally expected to be much larger for a cluster than for a group population at this luminosity limit.

Another significant difference between groups and clusters is their dwarf-to-giant ratio (Ferguson & Sandage 1991). In our case we get (dE&dS0/E&S0) = 0.81 and (Im&BCD/Sp) = 0.57 for Cen30 and (dE&dS0/E&S0) = 0.24 and (Im&BCD/Sp) = 0.52 for Cen45, respectively. In terms of environmental differences these numbers are comparable to the Fornax cluster and the Leo group at our luminosity limit $M_{BT} = -15.5$ (cf. Ferguson & Sandage 1991).

In Fig. 4 the velocity histograms for different Hubble types are shown. Intermediate types as e.g. S0/Sa were divided with half weight to both types. E&S0 galaxies populate the range $1700\text{--}5300 \text{ km s}^{-1}$ smoothly with no obvious centre. In contrast, the dE&dS0s which are mostly nucleated dwarf ellipti-

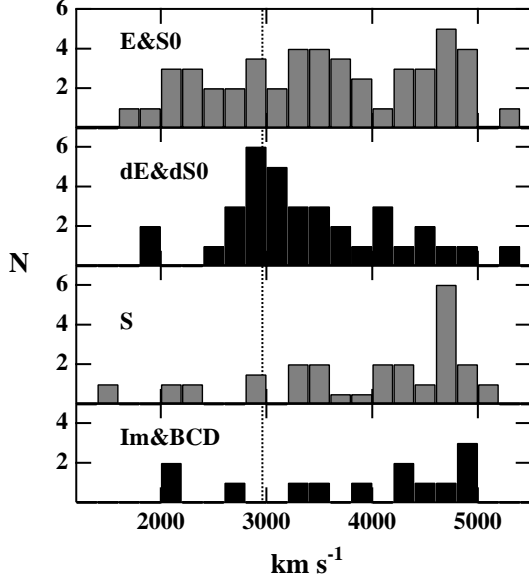


Fig. 4. The velocity distributions of the Centaurus cluster binned into different Hubble types. The dotted line indicates the redshift of the brightest cluster galaxy NGC 4696

Table 4. Type mixtures for the two cluster velocity components

Type (1)	Cen30		Cen45	
	number (2)	% (3)	number (4)	% (5)
E	14.17	14	2.32	11
S0	26.31	27	5.69	27
Spirals	16.21	16	7.29	34
Im&BCD	9.21	9	3.79	18
dE&dS0	33.10	33	1.90	10
All	99.00	100	21.00	100

icals are highly concentrated. A least-squares fit of a Gaussian profile gives $\mu_{dE&dS0}=3148\pm 98 \text{ km s}^{-1}$ with a velocity dispersion of $\sigma_{dE&dS0}=530\pm 88 \text{ km s}^{-1}$. There is a remarkable coincidence between the derived mean velocity and the central velocity of the Cen30 cluster component and in particular with the velocity of NGC 4696. This strongly suggests a dynamical link between these bright early-type dwarfs and the cluster potential and/or the dominant galaxy in Cen30. We will investigate this issue in Section 6 in more detail. It has been claimed that the dE&dS0s galaxy class is the most strongly clustered of all (e.g. Vader & Sandage 1991). Our result from the third dimension (velocity) is a full confirmation of this 2D-based conclusion.

Like the E&S0s, the cluster spirals are also distributed over the a large velocity range 1400-5200 km s^{-1} . However, in this case there is a slight preference to velocities higher than 4000 km s^{-1} (median value 4350 km s^{-1} with a peak at 4700 km s^{-1}). Below the median velocity each bin contains an average galaxy number of 0.8. Above this velocity the value is 2.5 times higher. The velocity distribution of our late-type dwarf sample com-

pares very well with that of the spirals. Their distribution is flat covering the range 2000-5000 km s^{-1} without any obvious concentration. The median velocity of the whole sample is 4300 km s^{-1} .

6. Bound companions

A remarkable feature of Fig. 4 is that most early type dwarfs are distributed with a nearly Gaussian-like shape around a velocity of about 3000 km s^{-1} with a significantly smaller velocity dispersion than the cluster itself. This rises the question of whether there is a population of dynamically bound satellites around NGC 4696. Note that while the general presence of bound companion galaxies in clusters has been convincingly proven (Ferguson 1992), there is still uncertainty about whether these satellites are mainly bound to central dominant galaxies or not (Gebhardt & Beers 1991; Merrifield & Kent 1991, and references therein).

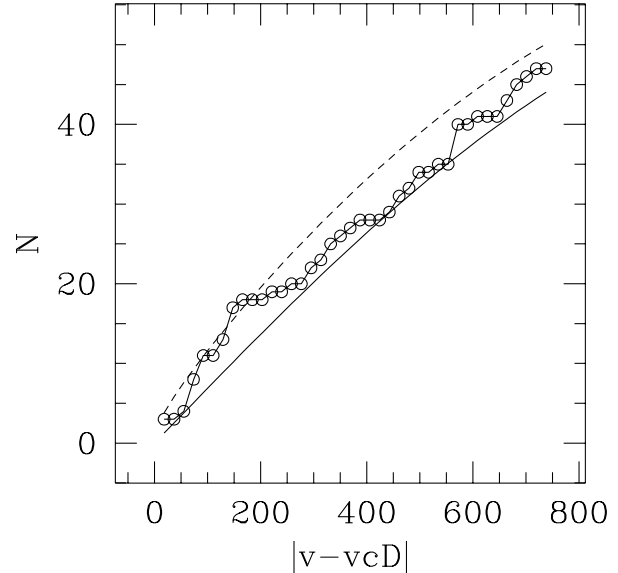


Fig. 5. “Indicator” Test for the presence of bound galaxies around NGC 4696. The number of galaxies found below a given velocity difference (circles), resp. expected in the mean (continuous line) and at most (95 % level, dashed line) is plotted against the velocity difference relative to NGC 4696. Only early type galaxies with $cz < 4250 \text{ km s}^{-1}$ have been included in the analysis.

To assess the significance of the overabundance of low-velocity galaxies around NGC 4696, we applied a slightly modified version of the “Indicator” Test (Gebhardt & Beers 1991). This test compares the number of galaxies in a range of velocities around the central galaxy with the number expected if they were drawn from the overall cluster (Gaussian) velocity distribution.

Because of the bimodal velocity distribution of Centaurus, and given that late types are not expected to be normally distributed, we selected those 65 galaxies of types E, S0, dE, dS0 with velocities less than 4250 km s^{-1} as pertaining to Cen30. We then specified the main population of Cen30 as being drawn from a Gaussian with parameters taken from Table 2, column 3, and computed the “Indicator” statistic, taking into account the incompleteness above 4250 km s^{-1} . See Fig. 5 for a graphical representation of the “Indicator” Test.

The test confirms that those galaxies with radial velocities differing by less than about 200 km s^{-1} from NGC 4696 have a 2σ probability of not being drawn from the overall cluster velocity distribution. This value is reasonable if it refers to a sample of bound galaxies, because it lies below what has been measured for the stellar velocity dispersion of NGC 4696 itself, i.e. 256 km s^{-1} (Carollo et al. 1993). It can further be seen that for a velocity difference smaller than 200 km s^{-1} the number of galaxies found is in excess by about 6 with respect to the Gaussian hypothesis. Considering that our sample contains of the order of 100 galaxies in Cen30, there is a good agreement with Merrifield & Kent’s (1991) findings that 5 % of the galaxies are bound.

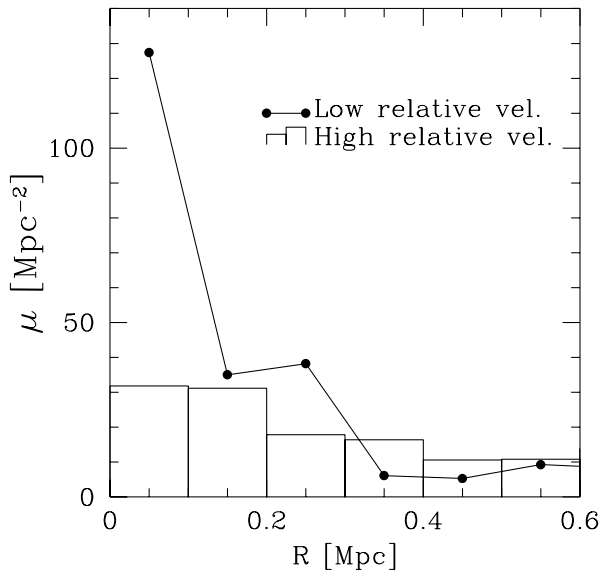


Fig. 6. Rough surface density profiles for sample galaxies with $|v_{\text{NGC 4696}} - v| > 250 \text{ km s}^{-1}$ (histogram) and $< 250 \text{ km s}^{-1}$ (line), respectively. Projected distance R of each galaxy to NGC 4696 has been calculated assuming a Hubble constant $H_0 = 50 \text{ km s}^{-1} \text{ Mpc}^{-1}$. Densities have been normalized to the same number of galaxies in both samples.

Note, however, that the results from the “Indicator” statistic are only true under the assumption that the moments of a Gaussian are good estimates for the cluster velocity distribution. In particular, this test is sensitive to the value of the dispersion for the underlying Gaussian, which is affected by relatively

large uncertainties. For this reason we compared also mean projected separations from NGC 4696 of candidate bound companion galaxies with other cluster members. Given that the sample of bound companion candidates has been selected based on redshift information only, this procedure gives an independent, qualitative check of the assumption. The reader might judge about the degree of concentration of the two samples towards the central dominant galaxy with the help of Fig. 6, where rough surface density profiles are shown for both samples. A correction for incompleteness below $RA = 12^{\text{h}} 44^{\text{m}}$ has been applied, and the densities have been normalized to the number of galaxies in the richer sample. In fact, the two histograms diverge appreciably for $R < 100 \text{ kpc}$, i.e. galaxies with lower relative velocity are preferably located closer to the dominant galaxy.

7. Summary and conclusions

The present redshift survey focused on the central region of the Centaurus galaxy cluster. Our aim was to investigate the nature of the reported bimodal structure in its velocity distribution. For this purpose we observed redshifts for a highly complete and deep sample of Centaurus cluster galaxies including a substantial number of dwarfs. Since dwarf galaxies show a more extreme behaviour with respect to the environment than giants, they offer a powerful diagnostic for the underlying conditions. We found significant differences in the velocity distributions of individual Hubble-types. The dwarf ellipticals are the only galaxies which are strongly clustered in velocity with a Gaussian-like distribution at a mean redshift of $3148 \pm 98 \text{ km s}^{-1}$ comparable to the centre of Cen30. This indicates that this galaxy type is carrying information about the mass distribution of a galaxy compound. Our results support the conclusions of earlier works (e.g. Vader & Sandage 1991) that dwarf ellipticals are the most clustered galaxy type.

We analysed the prominent bimodal velocity distribution of the complete sample. Dynamical properties of the two velocity components give evidence that the galaxies associated to Cen30 represent a real galaxy cluster at $v \sim 3400 \text{ km s}^{-1}$ whereas Cen45 must be a loosely bound system. Predictions based on the morphology-density relation for galaxies offered a test for this conclusion. We carried out a statistical analysis of the type-mixture of Cen30 and Cen45 galaxies which confirms the very different nature of the two aggregates. The true cluster is Cen30 with a large velocity dispersion of $933 \pm 118 \text{ km s}^{-1}$ and a high fraction of early-type galaxies. On the other hand, Cen45 is a late-type galaxy dominated system with a very low velocity dispersion of only $131 \pm 43 \text{ km s}^{-1}$ comparable to a poor galaxy group. With respect to their dwarf-to-giant ratios the velocity components are as different as the Fornax cluster and the Leo group. The issue about the spatial location of the two components is not in reach of the present study and is generally hard to solve because of an intrinsic problem: Centaurus cluster samples are typically dominated by Cen30 galaxies. In our Cen45 sample we have a statistical number of < 7 objects per

morphological type which is far away from being sufficient to get a good distance from e.g. the Tully-Fisher relation for spirals or the $D_n - \sigma$ relation for ellipticals. An additional problem is the increasing background contamination for samples taken from larger cluster areas which is discussed in more details in Jerjen & Dressler (1997b). Apparently, only with distances to individual galaxies it will be possible to answer the distance question. In fact, Dressler (1993) determined distances to six elliptical galaxies, 4 in Cen30 and 2 in Cen45 applying the surface brightness fluctuation method. The latter galaxies (CCC 130 and CCC 134) have high probabilities of being Cen45 members: 0.76 and 0.66, respectively. He found no significant distance difference between the six galaxies. This preliminary but important result combined with our results on the physical nature of Cen30 and Cen45 gives a consistent picture for the Centaurus cluster of a dynamically young, unrelaxed system which is still in the process of formation. Thereby the infalling galaxy group Cen45 represents a main subcomponent which might be close to the cluster centre and thus experience a high peculiar velocity.

In this paper, we have also investigated in detail on the very different velocity distribution of early-type dwarfs as compared to those of giant galaxies or Im&BCD dwarfs. The early-type dwarfs are highly concentrated towards the gravitational centre of the massive Cen30 in a Gaussian-like distribution. This stands in contrast to the results for the Virgo cluster, where dE&dS0s have a non-Gaussian velocity distribution (Ferguson 1992). This behaviour may give some clue to the physical processes responsible for the formation and evolution of dwarf ellipticals in clusters. Another signature for ongoing evolution in the cluster core is represented by the detection of a small bound population of early-type giant and dwarf galaxies around the central dominant galaxy of Cen30. As a strong hint that a few percent of the cluster galaxies are, in fact, bound either to NGC 4696 or to a peak in the cluster mass distribution, coinciding with the position of NGC 4696.

Acknowledgements. It is a pleasure to thank Dr. B. Binggeli for many comments and suggestions on the manuscript. We are grateful to the Swiss National Science Foundation for financial support.

References

- Binggeli, B., 1993, Habilitationsschrift, University of Basel
 Binggeli, B., Sandage, A., Tammann, G.A., 1987, AJ, 94, 251
 Binggeli, B., Tarenghi, M., Sandage, A., 1990, A&A, 228, 42
 Binggeli, B., Popescu, C.C., Tammann, G.A., 1993, A&AS, 98, 275
 Blakeslee, J.P., Tonry, J.L., 1992, AJ, 103, 1457
 Carollo, C.M., Danziger, I.J., Buson, L., 1993, MNRAS, 265, 553
 Cuby, J.-G., Mignoli, M., 1994, in "Instrumentation in Astronomy VIII" SPIE Conf. Ser. 2198, pag. 98
 Dickens, R.J., Currie, M.J., Lucey, J.R., 1986, MNRAS, 220, 679 (DCL)
 Dressler, A., 1980, ApJ, 236, 351
 Dressler, A., 1993, in "Cosmic Velocity Fields", Proceedings of the 9th IAP Astrophysics Meeting, eds. F.R. Bouchet and M. Lachièze-Rey, Editions Frontières, Gif-sur-Yvette, p. 9
 Dressler A., Faber S.M., Burstein D., Davies R.L., Lynden-Bell D., Terlevich R.J., Wegner G., 1987, ApJ, 313, L37
 Faber S.M., Wegner G., Burstein D., Davies R.L., Dressler A., Lynden-Bell D., Terlevich R.J., ApJS, 1989, 69, 763
 Felenbok, P. et al., 1997, Experimental Astronomy, 7, 65
 Ferguson, H.C., 1992, MNRAS, 255, 389
 Ferguson, H.C., Sandage, A., 1988, AJ, 96, 1520
 Ferguson, H.C., Sandage, A., 1991, AJ, 101, 765
 Gebhardt, K., Beers, T. C., 1991, ApJ, 383, 72
 Girardi, M., Biviano, A., Giuricin, G., Mardirossian, F., Mezzetti, M., 1993, ApJ, 404, 38
 Held, E.V., Mould, J.R., 1994, AJ, 107, 1307
 Horne K., 1986, PASP 98, 609
 Jerjen, H., 1995, PhD thesis, Astronomical Institute of the University of Basel, Switzerland
 Jerjen, H., 1997, in preparation
 Jerjen, H., Dressler, A., 1997a, A&AS, in press
 Jerjen, H., Dressler, A., 1997b, in preparation
 Jerjen, H., Tammann, G.A., 1997, A&A, 321, 713
 Jerjen, H., Freeman, K.C., Binggeli, B., 1997, in preparation
 Kraan-Korteweg R.C., Woudt P.A., Cayatte V., Fairall A.P., Balkowski C., Henning P.A., 1996, Nature, 379, 519
 Lissandrini C., Cristiani S., La Franca F., 1994, PASP, 106, 1157L
 Lucey, J.R., Carter, D., 1988, MNRAS, 235, 1177
 Lucey, J.R., Currie, M.J., Dickens R.J., 1986a, MNRAS, 221, 453 (LCD)
 Lucey, J.R., Currie, M.J., Dickens R.J., 1986b, MNRAS, 222, 427
 Lynden-Bell, D., Faber, S.M., Burstein, D., Davies, R.L., Dressler, A., Wegner, G., 1988, ApJ, 326, 19
 Merrifield, M.R., Kent, S.M., 1991, AJ, 101, 783
 Sandage, A., Binggeli, B., Tammann, G.A., 1985, AJ, 90, 1759
 Stein, P., 1996, A&AS, 116, 203
 Stein, P., 1997, A&A, 317, 670
 Tonry, J., Davis, M., 1979, AJ, 84, 1511
 Vader, J.P., Sandage, A., 1991, ApJ, 379, L1

Table 5a. New redshifts for Centaurus cluster members. Coordinates (1950.0) are given in columns 2 and 3, column 4 gives the Centaurus Cluster Catalogue (Jerjen & Dressler 1996a) reference number. The galaxy morphological type (5), the total blue magnitude (6) and effective surface brightness (7) are taken from this same source, while the probability of being Cen45 cluster member (8) has been derived in Section 5. Please note that if $\text{prob}_{45}=0.00$ this automatically implies that the galaxy is a 100% Cen30 member. Column 11 contains the heliocentric radial velocity (cz) and its estimated uncertainty, which results from a weighted average of columns 9 (cross-correlation redshift) and column 10 (emission line redshift).

Seq (1)	RA (2)	Dec (3)	CCC (4)	Type (5)	B_T (6)	SB_{eff} (7)	prob_{45} (8)	V_{ccf} (9)	V_{emi} (10)	V (11)
1	12 44 44.68	-41 22 39.0	1	dE,N	17.09	22.7	0.00	3527±59		3527±59
3	12 44 47.86	-40 51 33.0	6	Im	16.65	23.2	0.00		3848±50	3848±50
5	12 44 59.61	-40 52 59.0	11	dS0:N	17.75	23.3	0.00	2750±43		2750±43
7	12 45 03.75	-40 43 33.9	13	dS0,N	16.83	22.5	0.00	3026±29		3026±29
13	12 45 22.85	-41 35 26.0	32	Im	16.98	23.5	0.00	2737±28		2737±28
15	12 45 29.58	-41 26 36.0	38	dE,N	18.10	23.9	0.00	3925±45		3925±45
16	12 45 30.24	-41 02 35.0	41	Im	18.75	23.9	0.00		4278±58	4278±58
22	12 45 50.31	-41 10 02.9	58	dE	17.94	24.1	0.00	3304±60		3304±60
23	12 45 53.96	-40 59 44.0	61	dE,N	17.43	23.8	0.00	2910±67		2910±67
28	12 46 14.60	-40 42 02.0	73	SBm	16.90	23.6	0.88		4823±50	4823±50
30	12 46 16.08	-40 59 14.0	75	dE,N	18.06	23.2	0.00	1958±71		1958±71
34	12 46 23.88	-40 55 14.0	84	dS0	17.73	23.7	0.00	3122±29		3122±29
36	12 46 28.05	-41 27 32.9	88	dE,N	18.06		0.00	2848±26		2848±26
38	12 46 36.81	-40 58 58.0	91	dE	19.40	24.8	0.00	3652±61		3652±61
42	12 46 44.21	-41 08 55.0	97	dE,N	18.70	23.7	0.00	2818±30		2818±30
47	12 46 53.03	-41 32 14.0	109	Im	19.48	24.8	0.00	3545±60		3545±60
48	12 46 54.00	-41 05 38.9	111	dE,N	16.94	23.8	0.00	2880±40		2880±40
49	12 46 56.04	-40 57 23.9	113	E	17.33	22.6	0.00	3715±26		3715±26
52	12 47 06.75	-40 34 29.0	120	dS0	17.00	23.3	0.00	3106±28		3106±28
53	12 47 08.06	-41 04 03.0	121	Im	18.36	24.3	0.88	4739±70		4739±70
55	12 47 10.02	-41 07 43.9	123	dS0	18.45	24.0	0.82	4661±69		4661±69
56	12 47 10.38	-40 59 16.9	125	dE,N	17.14	23.8	0.00	2880±35		2880±35
64	12 47 34.73	-41 23 31.0	146	dE	17.77	23.7	0.00	2675±53		2675±53
65	12 47 37.96	-41 01 28.9	150	dE,N	18.23	24.5	0.13	4426±46		4426±46
71	12 48 12.00	-41 06 26.0	172	dE,N	18.21	24.6	0.86	4844±45		4844±45
72	12 48 12.65	-41 13 22.9	173	Im	18.30	24.1	0.00	2139±36		2139±36
82	12 48 51.43	-40 53 59.0	193	Sc	17.51	23.4	0.76	4924±56		4924±56
83	12 48 53.30	-41 12 39.0	196	Im	18.10	24.3	0.83		4879±58	4879±58
88	12 49 06.16	-41 26 10.0	209	dE	18.32	24.2	0.00	3535±76		3535±76
91	12 49 14.16	-40 52 15.0	212	Im	19.06		0.00	2085±39		2085±39
94	12 49 15.44	-41 08 49.9	215	dE	19.50	24.6	0.00	3329±76		3329±76
96	12 49 18.24	-40 38 05.9	219	Im	17.10	23.5	0.00		3284±71	3284±71
103	12 49 34.13	-41 28 48.0	228	dE,N	18.09	24.1	0.00	3212±62		3212±62
104	12 49 35.37	-40 53 47.0	230	Im	17.94	24.4	0.83		4881±45	4881±45
106	12 49 48.10	-40 57 16.0	239	Im	18.00	24.4	0.64		4971±71	4971±71
112	12 51 15.00	-41 07 31.0	277	Sc	16.54	22.1	0.17	4441±73		4441±73

Table 5b. New redshifts of background galaxies. Coordinates (1950.0) are given in columns 2 and 3, column 4 gives the Centaurus Cluster Catalogue (Jerjen & Dressler 1996a) reference number. The galaxy morphological type (5), the total blue magnitude (6) and effective surface brightness (7) are taken from this same source. Column 10 contains the heliocentric radial velocity (cz) and its estimated uncertainty, which results from a weighted average of columns 8 (cross-correlation redshift) and column 9 (emission line redshift).

Seq (1)	RA (2)	Dec (3)	CCC (4)	B_T (5)	SB_{eff} (6)	V_{ccf} (7)	V_{emi} (8)	V (9)
6	12 45 00.98	-40 56 44.0	12	18.82	24.4	38469±66		38469±66
14	12 45 26.04	-40 16 07.9	33	17.49	23.1	14702±81	14706±58	14705±47
18	12 45 36.96	-41 25 31.0	44	19.76	24.3		21123±50	21123±50
21	12 45 49.10	-41 27 29.9	56	18.90	24.8	13792±84		13792±84
29	12 46 15.02	-41 09 21.0	74	18.76	23.7	16514±64		16514±64
39	12 46 38.54	-40 21 50.0	92	17.70	23.5		10746±58	10746±58
57	12 47 14.58	-41 27 06.0	127	17.85	23.6	16362±45		16362±45
58	12 47 15.19	-41 10 30.0	128	19.28	24.2	46615±85		46615±85
63	12 47 31.28	-41 01 54.9	142	18.40	24.0	20843±56		20843±56
74	12 48 27.17	-40 32 34.9	179	17.27	22.6	14863±61	14878±58	14871±42
76	12 48 31.57	-41 00 13.0	182	18.01	23.3		10679±38	10679±38
77	12 48 41.55	-40 27 12.9	186	17.98	22.6	27387±91	27371±58	27376±49
92	12 49 14.18	-40 18 54.0	213	17.23	23.5	15916±44		15916±44
97	12 49 18.44	-41 22 21.0	220	17.93	23.1		19439±50	19439±50

Table 5c. Reobserved redshifts for Centaurus cluster members. Coordinates (1950.0) are given in columns 2 and 3, column 4 gives the Centaurus Cluster Catalogue (Jerjen & Dressler 1996a) reference number. The galaxy morphological type (5), the total blue magnitude (6) and effective surface brightness (7) are taken from this same source, while the probability of being Cen45 cluster member (8) has been derived in Section 5. Please note that if $\text{prob}_{45}=0.00$ this automatically implies that the galaxy is a 100% Cen30 member. Column 11 contains the heliocentric radial velocity (cz) and its estimated uncertainty, which results from a weighted average of columns 9 (cross-correlation redshift) and column 10 (emission line redshift).

Seq (1)	RA (2)	Dec (3)	CCC (4)	Type (5)	B_T (6)	SB_{eff} (7)	prob_{45} (8)	V_{ccf} (9)	V_{emi} (10)	V (11)
2	12 44 46.32	-40 59 22.0	4	S0	16.93	22.1	0.00	2704±61	2714±58	2709±42
4	12 44 56.98	-41 15 21.9	8	SB0	14.03	21.5	0.00	3531±25		3531±25
8	12 45 10.56	-40 38 53.0	17	S0	15.95	22.4	0.00	3874±70		3874±70
9	12 45 14.22	-40 56 49.2	19	d:S0	15.82	22.1	0.00	4059±19		4059±19
10	12 45 16.54	-41 01 57.5	22	dE	17.94	23.5	0.00	2433±33		2433±33
11	12 45 16.76	-40 19 19.0	24	SBd	15.21	22.5	0.00		4017±58	4017±58
12	12 45 19.01	-40 56 29.9	26	SBc	16.06	22.4	0.00	1414±77		1414±77
17	12 45 35.56	-41 26 28.9	43	S0	14.05	20.6	0.00	2647±25		2647±25
19	12 45 37.24	-40 51 03.2	45	E	14.93	20.8	0.00	3681±49		3681±49
20	12 45 45.33	-41 02 02.8	54	E	15.90	20.3	0.00	2958±44		2958±44
24	12 45 57.41	-41 22 15.9	62	S0	15.37	21.8	0.00	2193±19		2193±19
25	12 46 03.51	-41 02 18.9	65	E/S0	11.32	22.6	0.00	2985±31		2985±31
26	12 46 08.09	-41 02 48.0	70	E	15.64	18.3	0.00	2317±20		2317±20
27	12 46 09.66	-40 18 33.0	71	S0	14.76	21.3	0.00	3541±25		3541±25
31	12 46 17.22	-41 07 10.7	76	dS0	16.41	21.8	0.00	5298±28		5298±28
32	12 46 18.34	-41 03 59.9	77	Sc	15.99	23.2	0.00	3513±34		3513±34
33	12 46 20.34	-41 33 35.9	80	S0	14.78	21.8	0.13	4422±23		4422±23
35	12 46 26.03	-41 16 21.5	85	SBa	15.07	22.5	0.00	2839±20		2839±20
37	12 46 32.63	-41 03 48.0	89	E	15.77	20.0	0.00	3104±19		3104±19
40	12 46 39.53	-41 09 25.0	94	dS0,N	16.67	23.2	0.00	4076±29		4076±29
41	12 46 40.18	-41 13 03.0	95	SB0	14.56	21.7	0.00	4222±21		4222±21
43	12 46 46.81	-41 37 43.0	102	S0	14.65	22.4	0.00	3347±23		3347±23
44	12 46 48.55	-40 46 59.0	103	S0	14.41	20.4	0.00	1990±24		1990±24
45	12 46 51.82	-41 06 57.1	106	SB0/a	14.62	21.7	0.00	3677±19		3677±19
46	12 46 52.56	-40 48 58.7	108	E	16.11	19.9	0.00	3263±36		3263±36
50	12 46 56.15	-40 24 51.9	114	SBb	15.78	23.0	0.00	2242±24		2242±24
51	12 47 05.57	-40 57 14.0	119	E	14.64	20.3	0.00	2101±23		2101±23
54	12 47 08.12	-41 00 26.3	122	S0/a	14.18	21.6	0.00	3845±23		3845±23
59	12 47 17.90	-41 06 35.9	130	E	12.43	22.6	0.76	4624±25		4624±25
60	12 47 21.59	-41 07 32.9	134	E	15.04	20.6	0.66	4966±31		4966±31
61	12 47 25.40	-40 56 57.2	135	E	15.35	20.6	0.00	2908±26		2908±26
62	12 47 26.12	-41 14 36.0	137	S0	14.03	20.4	0.00	2384±24		2384±24
66	12 47 38.33	-40 34 26.9	151	Sa	14.27	22.2	0.79	4640±20		4640±20
67	12 47 48.05	-41 11 58.0	158	S0	14.77	21.3	0.01	5249±24		5249±24
68	12 48 00.14	-41 37 20.9	165	S0	14.87	20.7	0.89	4758±25		4758±25
69	12 48 11.13	-41 07 28.9	170	S0	15.24	20.4	0.25	4466±19		4466±19
70	12 48 11.30	-40 36 53.0	171	BCD	16.76	22.3	0.60	4562±22		4562±22
73	12 48 14.65	-41 27 01.9	175	E	14.65	21.7	0.00	2469±23		2469±23
75	12 48 31.55	-40 32 50.0	181	SB0	14.76	21.8	0.00	3391±23		3391±23
78	12 48 42.69	-41 34 20.9	187	d:S0	15.99	22.3	0.00	1826±19		1826±19
79	12 48 46.40	-40 57 21.5	189	Sc	15.02	21.3	0.89	4771±24		4771±24
80	12 48 49.76	-41 13 14.4	190	dS0,N	16.11	21.7	0.00	4048±23		4048±23
81	12 48 50.78	-41 01 54.7	191	S0	15.32	21.1	0.00	3467±22		3467±22
84	12 48 59.52	-40 59 42.7	203	dS0	16.72	21.7	0.08	4400±20		4400±20
85	12 49 01.57	-40 43 19.9	205	S0	15.95	22.1	0.00	2563±47		2563±47
86	12 49 04.27	-40 54 52.8	207	E	16.01	21.0	0.87	4712±18		4712±18
87	12 49 04.70	-41 09 38.3	208	dE,N	17.44	23.3	0.00	3624±22		3624±22
89	12 49 09.74	-41 16 02.8	210	SB0	15.16	21.7	0.00	3675±19		3675±19

(cont.)

Seq (1)	RA (2)	Dec (3)	CCC (4)	Type (5)	B_T (6)	SB_{eff} (7)	prob ₄₅ (8)	V_{cef} (9)	V_{emi} (10)	V (11)
90	12 49 13.97	-40 52 32.2	211	S0	14.09	22.1	0.00	2025±26		2025±26
93	12 49 14.56	-41 00 28.0	214	Sc	14.73	22.6	0.89	4806±32	4757±50	4792±27
95	12 49 16.48	-41 11 17.6	217	SB0	14.04	21.1	0.00	3950±22		3950±22
98	12 49 26.21	-41 04 02.8	222	Sc	14.74	23.2	0.17	5107±31		5107±31
99	12 49 28.70	-41 12 19.0	224	dS0	16.49	23.5	0.00	3037±26		3037±26
100	12 49 29.06	-40 59 15.5	225	S0	15.71	22.5	0.00	3459±23		3459±23
101	12 49 29.31	-41 07 08.6	226	S0/a	14.08	21.7	0.00	2968±23		2968±23
102	12 49 33.02	-40 47 22.0	227	SBa	13.60	22.2	0.00	3389±26		3389±26
105	12 49 39.54	-40 26 13.0	236	SB0	14.32	22.0	0.18	4445±21		4445±21
107	12 49 54.27	-40 57 31.0	242	S0	15.46	19.3	0.85	4858±23		4858±23
108	12 50 18.65	-40 33 13.9	255	S0	15.92	20.6	0.87	4831±22		4831±22
109	12 50 27.27	-40 52 10.6	260	dE,N	17.59	23.9	0.00	2766±43		2766±43
110	12 50 39.31	-40 55 59.9	266	E	13.08	21.4	0.01	4314±23		4314±23
111	12 50 55.53	-40 45 32.0	272	Im/BCD	16.51	23.0	0.00	4215±48		4215±48
113	12 51 19.19	-40 37 47.9	279	S0	15.67	20.7	0.00	3024±17		3024±17
114	12 51 41.30	-40 53 12.0	284	Sd	15.86	21.7	0.02	4367±41	4319±58	4351±34
115	12 52 10.47	-40 42 48.9	290	E	16.31	21.7	0.02	4344±19		4344±19